3D Visual Servoing from Uncalibrated Cameras for Uncalibrated Robots

Jun Adachi Jun Sato
Department of Electrical and Computer Engineering
Nagoya Institute of Technology
Nagoya 466-8555, Japan

Abstract

The visual servoing is very useful for navigating robots toward goal positions and orientations reliably. Unfortunately, the existing methods require calibration of cameras and robots. It is very difficult to calibrate cameras and robots accurately and reliably. Thus, in this paper, we propose a method which enables us to navigate uncalibrated robots to goal positions by using uncalibrated cameras. In particular, we show that projective invariants defined by the epipolar geometry can be exploited for navigating uncalibrated robots toward goal positions reliably. The proposed method is implemented and tested in real time visual servoing experiments.

Keywords: *visual servoing, uncalibrated cameras, uncalibrated robots, epipolar geometry, projective invariants.*

1. Introduction

The visual servoing is a method for controlling robots with cameras to arbitrary goal positions by using the difference between current images and goal images. It enables us to control robots reliably, even if the goal positions move during servoing.

The existing visual servoing methods can be divided into two groups [7], i.e. position based methods [1, 2, 8] and image based methods [5, 4]. The position based methods first reconstruct three dimensional configurations of the scene, and then control robots to the goal positions. These methods can generate the shortest path to goal positions. However, they require three dimensional reconstruction of the scene.

The image based methods, on the other hand, exploit changes in images directly for feedback gains for controlling robots to goal positions, and thus do not require three dimensional reconstruction. However, they cannot use three dimensional configurations of current and goal positions, and thus they do not generate optimum path in general [5]. To cope with this problem, the epipolar geometry has been used to divide robot motions into translational and rotational components, and to control robots to goal directions directly [3].

Unfortunately, these methods require the calibration of robots and cameras. That is we have to know internal and external parameters of cameras before servoing robots. Also we have to know the relationship between the control values and the three dimensional motions of robots. However, in general the real robots do not move as they are calibrated. For example, as shown in Fig. 1, three basis axes of many robots are not orthogonal each other, even if they are calibrated. Thus, the calibration of robots and cameras is, in general, very difficult. Recently, it has been shown that by using the epipolar geometry it is possible to navigate uncalibrated robots from uncalibrated cameras [12]. Unfortunately, the method is limited for controlling mobile robots which move on a plane.

In this research, we propose a method for navigating uncalibrated robots with three dimensional translational motions from uncalibrated cameras. Since uncalibrated robots with three dimensional motions have non-orthogonal three basis axes, it is very difficult to compute the proper ratios of control values for these three axes for navigating robots to goal positions.

To cope with this problem, we consider two projective spaces. That is the projective space defined by control values for robots, and the projective space defined by the epipolar geometry. By extracting the relationship between these two projective spaces, we derive control values for navigating uncalibrated robots to goal positions.

In section 2, we first set our problem of uncalibrated visual servoing. We next apply the epipolar geometry for identifying goal positions in images in section 3. We next show how the uncalibrated robots can be navigated toward goal positions from uncalibrated image information in section 4. Finally, we show the results of some real time visual servoing experiments.

2. Uncalibrated Visual Servoing

In this research, we assume that robots move in the 3D space, but has only three degrees of freedom in translational motions. Let $\mathcal{X}_1$, $\mathcal{X}_2$, $\mathcal{X}_3$ be the three

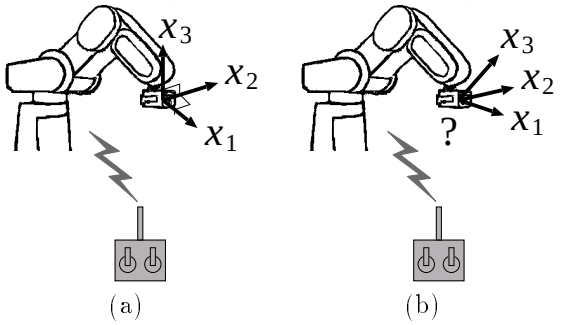

Figure 1. Calibrated robots and uncalibrated robots.

translational axes of robots. If the robots are perfectly calibrated, then these three axes are orthogonal each other as shown in Fig. 1 (a), and we know the relationship between the motions of robots and their control values. However, if the robots are uncalibrated or not perfectly calibrated, then these three axes, $\mathcal{X}_1$, $\mathcal{X}_2$, $\mathcal{X}_3$ are, as shown in Fig. 1 (b), not orthogonal in general, and the relationship between the robot motions and control values are unknown. That is, we do not know the direction of motions and the amount of motions caused by a unit translational commands. These are the uncalibrated robots which we assume in this research. The only assumption on robots is that a fixed amount of control values causes a fixed amount of robot motions.

The uncalibrated cameras are fixed on uncalibrated robots. Thus, the relative positions and orientations between cameras and robots are unknown. Also, the internal parameters of cameras are unknown.

Under these conditions, we propose a method for navigating robots toward goal positions reliably from uncalibrated cameras.

3. Epipolar Geometry and Visual Servoing

In this section, we describe how to derive useful information for navigating robots from uncalibrated cameras.

As it is well known, even if the cameras are uncalibrated, relative positions and orientations between two views can be extracted from images as the epipolar geometry [9]. In this section, we describe how the epipolar geometry can be exploited for navigating robots toward goal positions. To do this, we first review the epipolar geometry under translational motions.

3.1. Epipolar Geometry Under Translations

Let us consider a pair of corresponding points, $\mathbf{m} = [\,u \quad v\,]^\top$, $\mathbf{m}' = [\,u' \quad v'\,]^\top$, in images at two viewpoints, C, C'. Then, the relationship between these two points

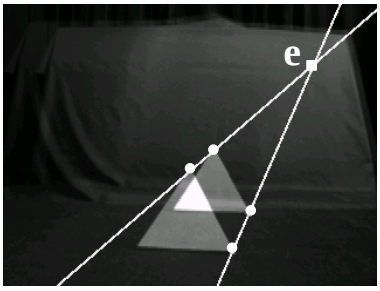

Figure 2. Epipolar geometry of translational cameras. These are two consecutive images taken before and after a translational motion. The epipolar lines and the epipoles coincide in these two views. Thus, epipolar lines can be extracted by simply drawing lines which go through corresponding points, and epipoles can be extracted as intersections of these epipolar lines.

can be described by the following epipolar equation:

$$\tilde{\mathbf{m}}'^\top \mathbf{F} \tilde{\mathbf{m}} = 0 \tag{1}$$

where, $(\tilde{})$ denotes homogeneous coordinates, and $\mathbf{F}$ denotes fundamental matrix. The matrix $\mathbf{F}$ can be computed linearly [6] or non-linearly [13]. It is known that $\mathbf{F}$ can be decomposed into two epipoles, $\mathbf{e}$, $\mathbf{e}'$, and an epipolar homography, $\mathbf{H}$ as follow [11]:

$$\mathbf{F} = \begin{bmatrix} \mathbf{L}^{-1}\mathbf{H} & -\mathbf{L}^{-1}\mathbf{H}\mathbf{e} \\ -\mathbf{e}'^\top \mathbf{L}^{-1}\mathbf{H} & \mathbf{e}'^\top \mathbf{L}^{-1}\mathbf{H}\mathbf{e} \end{bmatrix} \tag{2}$$

where, $\mathbf{L}$ is the following matrix:

$$\mathbf{L} = \begin{bmatrix} 0 & -1 \\ 1 & 0 \end{bmatrix} \tag{3}$$

Furthermore, if the camera motions are pure translations and if the camera internal parameters are unchanged under camera motions, the matrix $\mathbf{F}$ has the following form:

$$\mathbf{F} = \begin{bmatrix} 0 & -f_1 & f_2 \\ f_1 & 0 & -f_3 \\ -f_2 & f_3 & 0 \end{bmatrix} \tag{4}$$

In this case $\mathbf{F}^\top = -\mathbf{F}$, and thus two epipoles coincide each other. Also, the epipolar homography can be described by an identity matrix, and its degrees of freedom is 0. Thus, epipolar lines in two views also coincide each other. This is called the auto epipolar [10]. Fig. 2 shows two consecutive images taken before and after a translational motion, and shows that epipolar lines and epipoles coincide in these two images.

Since the fundamental matrix has scale ambiguity, it has, in this case, just two degrees of freedom which corresponds to the coordinates of a single epipole. This means that the epipolar geometry can be computed just from two corresponding points as shown in Fig. 2.

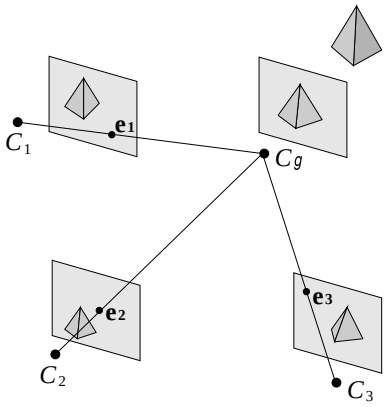

Figure 3. Goal positions and epipoles. C_1, C_2, C_3 **are current camera positions, and** C_g **is a goal camera position. The goal position can be observed as epipoles,** e_1, e_2, e_3, **in current images.**

3.2. Epipolar Geometry for Visual Servoing

The epipolar geometry is very important for visual servoing. Let us consider a goal position, C_g, and a current position, C, of the camera under visual servoing. If we compute epipoles, $\mathbf{e}$ and $\mathbf{e}'$, from images viewed at these two positions, the epipole, $\mathbf{e}$, in a current image shows the goal position, C_g, viewed at the current camera position, C. Thus, by controlling robots toward the direction of epipoles, $\mathbf{e}$, we can navigate robots to goal positions, C_g, from arbitrary positions, C, as shown in Fig. 3.

In general we need at least seven corresponding points to compute fundamental matrices. However, since we assume that the robot causes no rotational motions, we can compute fundamental matrices just from two corresponding points as shown in section 3.1. If we have more corresponding points, the epipoles can be computed more accurately from these points.

4. Visual Control of Uncalibrated Robots

As shown in section 3, we need to control robots toward the direction of epipoles for navigating robots to goal positions. However, since the robots are uncalibrated, we do not know how much control values are required for each axes, $\mathcal{X}_1$, $\mathcal{X}_2$, $\mathcal{X}_3$, to control robots toward the direction of epipoles. In this section, we propose a method for computing control values for each axes to control uncalibrated robots toward goal directions.

4.1. Epipolar Geometry and Projective Bases

To solve this problem, we consider projective spaces defined by control values for robots and epipoles in images. Let us first consider a three dimensional control space, $\mathcal{Y}$, defined by control values, $\mathbf{Y}^3 = [Y_1, Y_2, Y_3]^\top$, for three axes. The single control value, $\mathbf{Y}^3$, for a robot motion can be considered as a point in the control space, $\mathcal{Y}$. If the robot moves to a point, $\mathbf{C}^3 = [X, Y, Z]^\top$, in the real three dimensional space, $\mathcal{R}$, by a control value, $\mathbf{Y}^3$, then $\mathbf{C}^3$ and $\mathbf{Y}^3$ have the following relationship:

$$\widetilde{\mathbf{C}}^3 = \mathbf{A}_{4\times4}\widetilde{\mathbf{Y}}^3 \tag{5}$$

where, $\mathbf{A}_{4\times4}$ denotes a 4×4 affine matrix. This is because we have assumed that fixed amount of control values cause fixed amount of robot motions, and hence the distortion of motions of uncalibrated robots can be described by three dimensional affine transformations.

If we send control values, $\mathbf{Y}^3$, so that they are on a plane, Σ, in the control space, $\mathcal{Y}$, the robot positions, $\mathbf{C}^3$, caused by $\mathbf{Y}^3$ are also on a plane, Π, in the real space, $\mathcal{R}$, as shown in Fig. 4. Let $\mathbf{Y}^2$ be the two dimensional coordinates of point $\mathbf{Y}^3$ on the plane Σ, and $\mathbf{C}^2$ be the two dimensional coordinates of point $\mathbf{C}^3$ on the plane Π. Then, the relationship between $\mathbf{Y}^2$ and $\mathbf{C}^2$ can be described by planar affine transformations as follows:

$$\widetilde{\mathbf{C}}^2 = \mathbf{A}_{3\times3}\widetilde{\mathbf{Y}}^2 \tag{6}$$

where, $\mathbf{A}_{3\times3}$ denotes a 3×3 matrix for planar affine transformations. Such control values can be produced, for example, by choosing a fixed amount of control value for $\mathcal{X}_3$ axis. Thus, if we know the affine matrix, $\mathbf{A}_{3\times3}$, then we can compute control values, $\mathbf{Y}^2$, for controlling robots to arbitrary positions, $\mathbf{C}^2$, on Π. However, robots are uncalibrated, and thus matrix $\mathbf{A}_{3\times3}$ is unknown. In the following part of this paper, we use $\mathbf{Y}$ for $\mathbf{Y}^2$ and $\mathbf{C}$ for $\mathbf{C}^2$ for simplicity. Also, we use $\mathbf{A}$ for $\mathbf{A}_{3\times3}$.

If we compute epipolar geometry between two images taken before and after robot motions, the positions of cameras after robot motions can be observed as epipoles, $\mathbf{e}$, in images before robot motions. Since epipoles, $\mathbf{e}$, are the projection of camera positions, $\mathbf{C}$, on plane Π, the relationship between $\mathbf{e}$ and $\mathbf{C}$ can be described by planar projective transformations as follow:

$$\widetilde{\mathbf{e}} \sim \mathbf{P}\widetilde{\mathbf{C}} \tag{7}$$

where, $(\sim)$ denotes equality up to a scale. Thus, if we know the relationship, $\mathbf{P}$, between epipoles, $\mathbf{e}$, on a image plane, π, and camera positions, $\mathbf{C}$, on a plane, Π, in the real space, we can compute camera positions, $\mathbf{C}$, from epipoles, $\mathbf{e}$. However, we do not know $\mathbf{P}$, since cameras are also uncalibrated.

By substituting (6) into (7), we find that the relationship between control values, $\mathbf{Y}$, and epipoles, $\mathbf{e}$, can be described by planer projective transformations as follows:

$$\widetilde{\mathbf{e}} \sim \mathbf{P}'\widetilde{\mathbf{Y}} \tag{8}$$

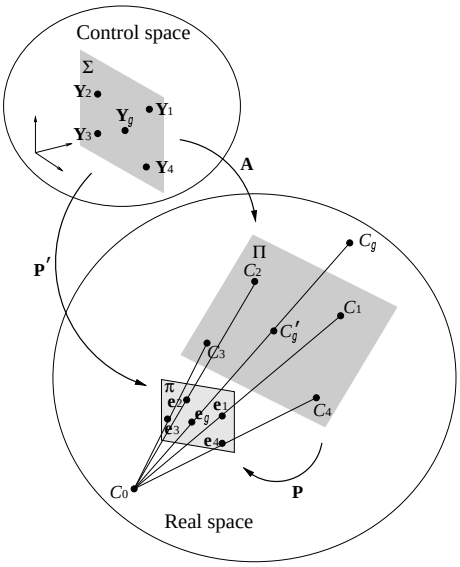

Figure 4. Relationship between control space and real space.

where, $\mathbf{P}' = \mathbf{PA}$. In the next section, we describe a method for controlling uncalibrated robots from this relationship.

4.2. Visual Control from Epipoles

For computing control values toward goal positions, we first send four control values, $\mathbf{Y}_i$ $(i = 1, \cdots, 4)$, which are on a plane, Σ, in the control space, $\mathcal{Y}$, as shown in Fig. 4. These control values can be generated by choosing a fixed amount of control values for one axis, e.g. $\mathcal{X}_3 = 1$. These control values can be considered as projective bases on a plane, Σ. Let $\mathbf{C}_i$ $(i = 1, \cdots, 4)$ be camera positions caused by control values, $\mathbf{Y}_i$, $(i = 1, \cdots, 4)$. Then, $\mathbf{C}_i$, $(i = 1, \cdots, 4)$ are also on a plane, Π, in the real space, as shown in Fig. 4. Note, Π is unknown. If we consider an intersection point, $\mathbf{C}'_g$, between Π and a line through current and goal camera positions, $\mathbf{C}$, $\mathbf{C}_g$, our task is to compute control values, $\mathbf{Y}_g$, for controlling robots to $\mathbf{C}'_g$ on Π.

Although we cannot compute $\mathbf{C}_1, \cdots, \mathbf{C}_4$ and $\mathbf{C}'_g$ directly, these points can be observed as epipoles, $\mathbf{e}_1$, $\cdots$, $\mathbf{e}_4$ and $\mathbf{e}_g$ in images. Since the relationship between $\mathbf{Y}$ and $\mathbf{e}$ is described by planar projective transformations, the invariants, $\mathcal{I}_Y$, computed from five points, $\mathbf{Y}_1, \cdots, \mathbf{Y}_4$, $\mathbf{Y}_g$, in the control space are equal to the invariants, $\mathcal{I}_e$, computed from five points, $\mathbf{e}_1, \cdots, \mathbf{e}_4$, $\mathbf{e}_g$ in images as follows:

$$\mathcal{I}_Y = \mathcal{I}_e \tag{9}$$

$$\mathcal{I}_Y = \frac{|\,\widetilde{\mathbf{Y}}_1 \;\; \widetilde{\mathbf{Y}}_2 \;\; \widetilde{\mathbf{Y}}_4\,||\,\widetilde{\mathbf{Y}}_1 \;\; \widetilde{\mathbf{Y}}_3 \;\; \widetilde{\mathbf{Y}}_g\,|}{|\,\widetilde{\mathbf{Y}}_1 \;\; \widetilde{\mathbf{Y}}_2 \;\; \widetilde{\mathbf{Y}}_3\,||\,\widetilde{\mathbf{Y}}_1 \;\; \widetilde{\mathbf{Y}}_4 \;\; \widetilde{\mathbf{Y}}_g\,|} \tag{10}$$

$$\mathcal{I}_e = \frac{|\,\widetilde{\mathbf{e}}_1 \;\; \widetilde{\mathbf{e}}_2 \;\; \widetilde{\mathbf{e}}_4\,||\,\widetilde{\mathbf{e}}_1 \;\; \widetilde{\mathbf{e}}_3 \;\; \widetilde{\mathbf{e}}_g\,|}{|\,\widetilde{\mathbf{e}}_1 \;\; \widetilde{\mathbf{e}}_2 \;\; \widetilde{\mathbf{e}}_3\,||\,\widetilde{\mathbf{e}}_1 \;\; \widetilde{\mathbf{e}}_4 \;\; \widetilde{\mathbf{e}}_g\,|} \tag{11}$$

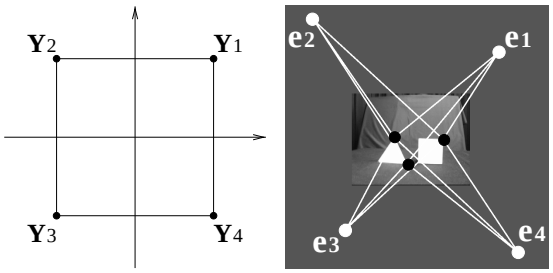

(a) plane Σ (b) image plane π

Figure 5. Four basis control values, $\mathbf{Y}_i$, given to the robot, and four basis epipoles, $\mathbf{e}_i$, extracted from images.

Thus, by using (9), (10) and (11), we can compute control values, $\mathbf{Y}_g$, toward goal positions from epipoles, $\mathbf{e}_1, \cdots, \mathbf{e}_4$, $\mathbf{e}_g$ and their control values, $\mathbf{Y}_1, \cdots, \mathbf{Y}_4$.

In this way, we can control robots toward goal positions efficiently, even if the robots and cameras are uncalibrated. The path caused by the proposed method is theoretically the shortest, since we can control robots to goal directions directly.

4.3. Distance Control

By using the proposed method described above, we can compute the ratio of control values, $\mathbf{Y}_g$, for three axes, $\mathcal{X}_1$, $\mathcal{X}_2$, $\mathcal{X}_3$, for controlling robots to goal directions. However, since epipoles do not have the information on distance, we do not know the magnitude of control values. Thus, we use the parallax in images as a measure of distance, and achieve the feedback control for distance.

If the robots are not at the goal positions, we have the difference, Δm, between goal and current images as follows:

$$\Delta m = \left(\frac{1}{N} \sum_{i=1}^{N} \Delta \mathbf{m}_i \Delta \mathbf{m}_i \right)^{\frac{1}{2}} \tag{12}$$

where, $\Delta \mathbf{m}_i$ denotes the difference in positions of ith feature points. By using Δm as feedback gain, we can achieve visual feedback control as follows:

$$\mathbf{Y}_g^k = \begin{cases} \lambda \Delta m^k \, \mathbf{Y}_g & (\Delta m^k \leq \Delta m^{k-1}) \\ -\lambda \Delta m^k \, \mathbf{Y}_g & (\Delta m^k > \Delta m^{k-1}) \end{cases} \tag{13}$$

where, $\mathbf{Y}_g^k$ is a set of control values at time k, and Δm^k is Δm at time k. λ denotes a fixed gain.

5. Experiments

We next show the results of some experiments exploiting the proposed method for navigating a real robot arm with a camera to goal positions.

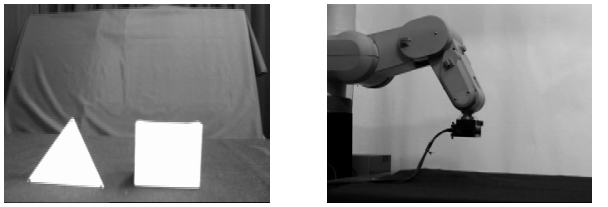

(a) image at goal position (b) robot at goal position

Figure 6. Camera image and robot at a goal position.

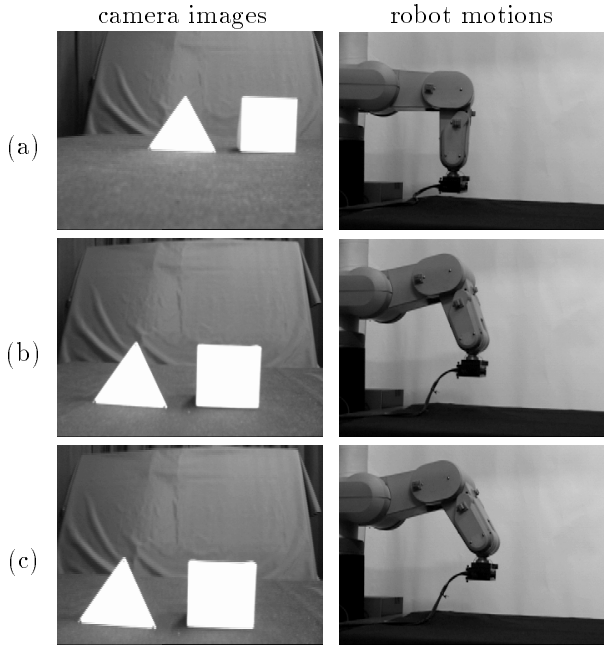

Figure 7. Results from the experiment of visual servoing. (a) shows a camera image and the robot at a start position. (b) shows those under visual servoing, and (c) shows those after visual servoing.

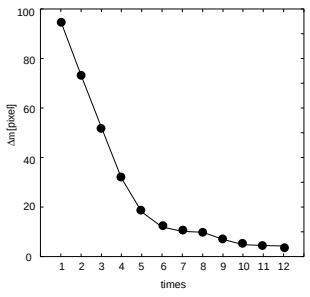

Figure 8. Changes in Δm under visual servoing.

5.1. Real Time Visual Servoing

As shown in Fig. 6 (b), a camera is fixed at the hand of a robot arm. Both the robot and the camera are uncalibrated. That is we do not know the relationship between control values and robot motions, and we do not know internal and external parameters of the camera. The image size is 320×240. The feature points in images are tracked by simple correlation trackers. Although the proposed method requires only two feature points, additional feature points can also be exploited for computing epipoles more accurately if they are available.

For controlling the uncalibrated robot from uncalibrated images, we first send four control values, $\mathbf{Y}_i$ $(i = 1, \cdots, 4)$, to the robot, and compute four epipoles, $\mathbf{e}_i$ $(i = 1, \cdots, 4)$, from images taken before and after robot motions. Then we navigate the robot toward goal positions by extracting epipoles, $\mathbf{e}_g$, of goal positions, and computing control values, $\mathbf{Y}_g$, toward $\mathbf{e}_g$. We continue the navigation until the difference, Δm, between current and goal images becomes smaller than a threshold value.

Fig. 5 (a) shows four control values, $\mathbf{Y}_i$ $(i = 1, \cdots, 4)$, given to the robot, and (b) shows extracted epipoles, $\mathbf{e}_i$ $(i = 1, \cdots, 4)$. The black dots in (b) show feature points used in this experiments, and white dots show extracted epipoles. Fig. 6 (a) and (b) show the camera image and the robot at a goal position.

Fig. 7 (a), (b), (c) show camera images and robot motions during visual servoing. The camera images are shown on the left, and robot motions are shown on the right. Fig. 7 (c) shows the results after the proposed visual servoing. As shown in Fig. 6 and Fig. 7 (c), the robot was navigated to the goal position reliably from the proposed method.

Fig. 8 shows changes in the difference, Δm, between the current and goal images under the visual servoing. We find that Δm converges to 0 monotonically.

5.2. Stability

We next show the stability of the proposed method. We navigated the robot from several different start positions, and evaluated the uncertainty bound of robot positions after visual servoing.

Fig. 9 (a) shows the stability of servoing from minimum number of feature points, i.e. two points. The square dots are start positions of the robot, and white dot is the goal position. The black dots show robot positions after visual servoing, and the ellipsoid shows an uncertainty bound with 3σ. It is elongated in the direction of Z axis, since it is the direction of camera axis and the parallax caused by the motion in this direction is smaller than those in other directions, The black lines are loci of the robot. As shown in this figure, the robot was navigated efficiently though almost the shortest path.

Fig. 9 (b) shows the results from seven feature points. From Fig. 9 (a) and (b), we find that the num-

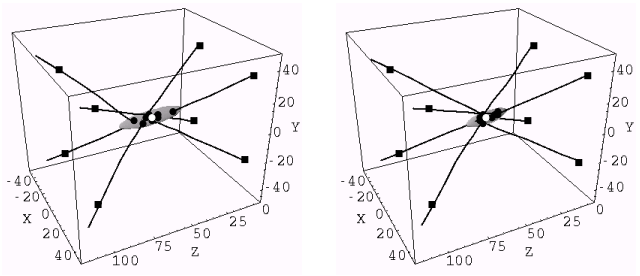

(a) (b)

Figure 9. Accuracy of visual servoing from two corresponding points.

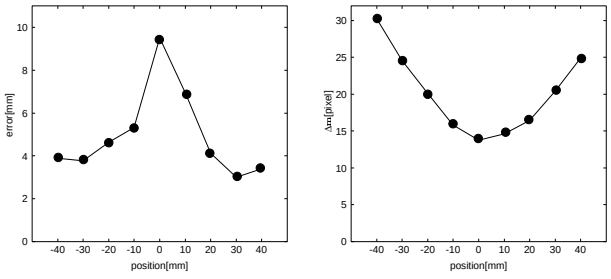

(a) errors in visual servoing (b) Δm at start positions

Figure 10. Start positions and the accuracy of visual servoing.

ber of feature points is important for stability of visual servoing.

We next evaluated the relationship between start positions and errors in visual servoing. Fig. 10 (a) shows the errors in camera position after visual servoing. The horizontal axis shows the distance between start positions and a camera axis at the goal position, and the vertical axis shows the errors in camera positions. Fig. 10 (b) shows the parallax, Δm, at start positions. As shown in (a), the visual servoing is inaccurate if the start positions are near the axis of camera at goal positions. This is because if the camera motion is close to the camera axis, the parallax, Δm, is small, and thus small image noises cause large errors in positioning.

6. Conclusion

In this paper we proposed a method for navigating uncalibrated robots to goal positions by using uncalibrated cameras.

We first showed that goal positions can be identified reliably by using the properties of auto epipolar, even if the cameras are uncalibrated. We next showed that by considering the projective space defined by control values and epipoles, the control values toward goal positions can be computed from images, even if the robots are uncalibrated. The proposed method was implemented and test by navigating an uncalibrated arm robot with an uncalibrated camera to goal positions in real time.

The proposed method is very useful for real visual servoing, since it is, in general, very difficult to calibrate robots and cameras accurately.

References

[1] P.K. Allen, A. Timcenko, B. Yoshimi, and P. Michelman. Automated tracking and grasping of a moving object with a robotics hand-eye system. *IEEE Trans. on Robotics and Automation*, 9(2):152–165, 1993.

[2] R. Cipolla and N. Hollinghurst. Visually guided grasping in unstructured environments. *Robotic and Automation Systems*, 19:337–346, 1997.

[3] K. Deguchi and R. Ishiyama. Optimal motion control for image-based visual servoing by decoupling translation and rotation. In *Meeting on Image Recognition and Understanding*, pages 337–343, 1998.

[4] K. Deguchi and T. Noguchi. Visual servoing using eigenspace method and dynamic calculation of interaction matrices. In *Proc. 13th International Conference on Pattern Recognition*, volume 1, pages 302–306, Vienna, Austria, August 1996.

[5] B. Espiau, F. Chaumette, and P. Rives. New approach to visual servoing in robotics. *IEEE Trans. Robotics and Automation*, 8(3):313–326, 1992.

[6] R.I. Hartley. In defense of the eight-point algorithm. *IEEE Trans. Pattern Analysis and Machine Intelligence*, 19(6):580–593, 1997.

[7] K. Hashimoto. *Visual Servoing –Real-Time Control of Robot Manipulators Based on Visual Sensory Feedback.* World Scientific Publishing, 1993.

[8] K. Kinoshita. Robot control using uncalibrated stereo and visual servoing. In *Proc. Meeting on Image Recognition and Understanding*, volume 2, pages 187–192, 1996.

[9] Q.T. Luong and O.D. Faugeras. The fundamental matrix: Theory, algorithm and stability analysis. *International Journal of Computer Vision*, 17(1):43–76, 1996.

[10] J.L. Mundy and A. Zisserman. Repeated structures: Image correspondence constraints and 3D structure recovery. In J.L. Mundy, A. Zisserman, and D.A. Forsyth, editors, *Applications of Invariance in Computer Vision*, pages 89–106. (LNCS 825), Springer–Verlag, 1994.

[11] J. Sato. *Computer Vision – Geometry of Vision –*. Corona Publishing, Tokyo, 1999.

[12] T. Sato and J. Sato. Visual servoing from uncalibrated cameras for uncalibrated robots. In *Proc. 4th Asian Conference on Computer Vision*, volume 2, pages 1162–1167, Taiwan, 2000.

[13] Z. Zhang. Determining the epipolar geometry and its uncertainty: A review. *International Journal of Computer Vision*, 27(2):161–195, 1998.